Cement and Concrete Research 178 (2024) 107438

Contents lists available at ScienceDirect

Cement and Concrete Research

journal homepage: www.elsevier.com/locate/cemconres

Multi technique characterization of the carbonation affected zone including non-destructive single sided ^{1}H NMR

Clarissa Glawe *, Fabien Georget, Michael Raupach, Thomas Matschei

Institute of building materials research Aachen (ibac), RWTH Aachen University, Schinkelstraße 3, 52062 Aachen, Germany

ARTICLE INFO

Keywords:
Building materials
Porosity
Carbonation
^{1}H NMR
Durability
Non-destructive testing
Corrosion

ABSTRACT

Carbonation of cement-based building materials is not only a frequent trigger for corrosion of the reinforcement, but also causes various significant property changes in the carbonated layer. In addition to the decrease in the pH of the pore solution, carbonation is accompanied by a modification in the pore structure due to dissolution and precipitation reactions. The progress of carbonation is currently commonly measured by the phenolphthalein test. In this study, the non-destructive unilateral hydrogen nuclear magnetic resonance (^{1}H NMR) was used to determine the carbonation progress of mortars as well as changes in the pore structure. The ^{1}H NMR results were correlated and validated with known methods for characterizing the carbonation progress, including the carbonation depths, but also other structural and mineralogical changes. These results serve as a proof-of-concept which gives reason to apply this non-destructive method to further building materials, especially new environmentally-friendly binders.

1. Introduction

The carbonation of concrete plays an important role both in the field of low CO_2 construction and in the preservation of structures. On the one hand, concrete has the ability to bind CO_2 from the atmosphere, which, in case of Portland cement, can result in reduced porosity while increasing strength. On the other hand, the transformation of the hydrate phases to form calcium carbonate ($CaCO_3$) leads to a lower pH of the pore solution in the carbonated area [1,2]. The pH reduction due to carbonation has a negative effect on the durability of reinforced concrete by causing a depassivation of the steel reinforcement and, later on, cracks and spalling on the component surface due to the increase in volume of the steel during corrosion. In contrast, the reduction of the total porosity causes a reduced moisture transport within the component and thus allows a reduction of the penetration of corrosion-promoting substances such as chlorides [3,4]. Regardless of which of the above two carbonation-based processes is considered, the change in the transport properties of the carbonated area plays a fundamental role in the durability of the structure [5].

Currently, the carbonation depth is usually determined with the color indicator phenolphthalein ($C_{20}H_{14}O_4$) indicating the transition point of a pH value below 8.2 of the surfaces to which it is applied [6]. However, it should be noted, that the carbonation is not a process characterized by a sharp boundary, but rather by a tortuous transition zone [7–9]. Starting from the high alkalinity of Portland cement (pH ~ 13), a pore solution with a pH of 11 already indicates a carbonation progress that would not be indicated with phenolphthalein [10]. Especially when alternative binders are used, the phenolphthalein test does not seem to be fully applicable when it comes to determining the real progress of the carbonation reaction [11]. Alternative binders, such as low-Calcium binders produced by supplementary cement materials (SCM) substitution using e.g. Metakaolin, seem to undergo a different carbonation process with respect to the development of the alkalinity of their pore solution, according to the current state of knowledge. Therefore, there is an additional need for new investigation methods for the carbonation of binders in the future.

While many studies have been conducted on the repair of carbonated structures by surface treatments or by restoring the alkalinity of the pore solution of the concrete, e.g. [12–14], new approaches that link the change in porosity, the resulting transport properties and the evolution of the phase composition of the material are in need [15–17]. By linking these properties, an improved understanding of the carbonation process can be achieved and thus new conditions for repair measures can be formulated and the possible applications of new binders expanded. Complementary to the determination of carbonation depth by the phenolphthalein test, there are several methods to investigate the

* Corresponding author.
E-mail address: glawe@ibac.rwth-aachen.de (C. Glawe).

https://doi.org/10.1016/j.cemconres.2024.107438
Received 26 June 2023; Received in revised form 18 December 2023; Accepted 21 January 2024
Available online 26 January 2024

change of cement-based materials during the carbonation process, such as XRD, TGA and FTIR [18–20]. In addition to their destructive character, they are all based on the analysis of prepared powder samples, which are limited in their result's accuracy by the precision of the extraction and preparation process. This leads to the fact that in the research work carried out to date with the above-mentioned methods, often only an approximation is made to the processes under consideration.

Initial attempts have been made to characterize accelerated carbonated cement-based structures using hydrogen nuclear magnetic resonance (^{1}H NMR) [7,21,22]. The method has yield very good results in the study of porous materials and polymers, making it a promising tool for in situ observation of building materials [23–30]. It was found that ^{1}H NMR offers a possibility to determine the carbonation depth of cement paste samples. In addition, ^{1}H NMR allows a more accurate characterization of the structural changes during the carbonation process with respect to the pore size distribution in water-saturated samples. As a result, the carbonated region of the studied system was divided into two layers, referred to as the carbonated layer and the transition zone [7]. The distinction of these zones is based on different relaxation times, which indicate a decrease in the total porosity in the carbonated layer, accompanied by a shift to larger pore sizes.

In contrast to previous publications, this work focuses on complementing the existing methods, including the phenolphthalein test rather than classifying it as inaccurate for the determination of the carbonation process. Using ^{1}H NMR, the present study aims to explain the carbonation depth given by the phenolphthalein test regarding the associated structural and mineralogical changes within the material during carbonation. This intends to associate the corrosion relevant turning point of the pore solution's pH value below 8.2 to an alteration process derived from the carbonation profile given by the ^{1}H NMR. Additionally, the potential of the ^{1}H NMR as a non-destructive method for the determination of the area affected by carbonation on various materials in the water saturated and non-saturated state is tested.

2. Materials and methods

In the first attempt to develop a suitable method, the choice of materials was intended to minimize the negative influences on the signal quality of the ^{1}H NMR. The measurement principle of ^{1}H NMR is based on the behavior of the hydrogen nuclei in the material under investigation as a result of an induced magnetic field. Therefore it is important to minimize other magnetic influences, such as the iron content of the material to be measured [31]. Accordingly, a white Portland cement (WPC) of the cement type CEM I was chosen, which is characterized, among other things, by a low iron oxide content (<0.25 %). The oxide composition obtained by XRF is shown in Table 1 as well as the phase composition, determined by XRD. The XRD measurement was carried out using a Panalytical X'Pert Pro X-Ray diffractometer equipped with a Panalyitcal X-Celerator detector. The analysis was done using the Bragg Brentano configuration and a X-ray tube (Cu Kα) at a voltage of 40 kV. The measurement range was 7 to 55°. As an internal standard, the cement sample was mixed with rutile powder (4:1) with a crystalline proportion of 94.38 %. The diffractogram pattern was evaluated with rietveld analysis which results in a proportion of amorphous components of 3.3 %. The phase composition by XRD is given in Fig. 1. Small amounts of Portlandite present in the raw cement can contribute to minor prehydration processes during the storage of the material before the preparation of the samples.

Table 1
Oxide and phase composition of the WPC used in this study.

Oxide	wt%	Phase	Proportion [%]
CaO	68.10	Alite	72.4
SiO_2	22.00	Belite	8.4
Al_2O_3	4.77	Aluminate	5.3
Fe_2O_3	0.22	Anhydrite	4.2
MgO	0.71	Bassanite	0.9
Na_2O	0.06	Portlandite	1.5
K_2O	0.74	Calcite	2.6
TiO_2	0.12	Lime	0.6
		Amorphous	4.1

2.1. Sample preparation

Mortar samples containing aggregates in form of norm sand with a w/b ratio of 0.50 and a binder to aggregate ratio of 0.29 were produced in the form of standard prisms (dimensions 40 × 40 × 160 mm^3) and slabs (dimensions 300 × 300 × 40 mm^3). As a proof-of-concept, further ^{1}HNMR measurements were performed on two concretes following the concrete class A4 according to [32]. Table 2 comprises the formulations and strengths of the two concretes and the white cement mortar after 28 days.

The specimens of the WPC were demolded 24 h after casting following storage under damp cloths and then stored in water for 6 days to ensure a proper curing of the sample, and avoid the creation of moisture gradients due to partial drying of the sample up to 7 days. It is assumed that the microstructure is mostly fixed at 7 days, even if the hydration continues slowly during the test. The water curing was followed by storage for 21 days at a relative humidity of 100 %.

Cores with a diameter of 50 mm and 100 mm and a height of 40 mm were extracted from the slabs by drilling and stored at a temperature of (21 ± 2) °C and a relative humidity of (65 ± 5) % for natural carbonation (0.05 %) for 10 months. It should be noted that carbonation under accelerated conditions (CO_2-Concentration > 3 %) causes different changes in the microstructure and possibly different reaction products compared to natural carbonation [16,33].

For the chemical investigations using Carbon-Sulfur Analysis (CSA – carbon and sulfur content quantification based on infrared analysis of volatiles after sample calcination) and Thermogravimetric Analysis (TGA), powder samples from a 100 mm diameter drill core were prepared and analyzed in 500 µm increments starting from the drill core surface to a depth of 5 mm. Fig. 2 shows a schematic diagram of the sample preparation for CSA and TGA analysis. In order to exclude an influence of the carbonated marginal areas, the drill cores (Ø = 100 mm) were overdrilled with a diameter of 80 mm. Subsequently, the depth-graded powder samples with a fineness of 125 µm were obtained by partial grinding of the sample in 500 µm steps.

In addition, thin sections were prepared covering the cross-section of the drill core with a diameter of 50 mm in 28 mm width and 48 mm

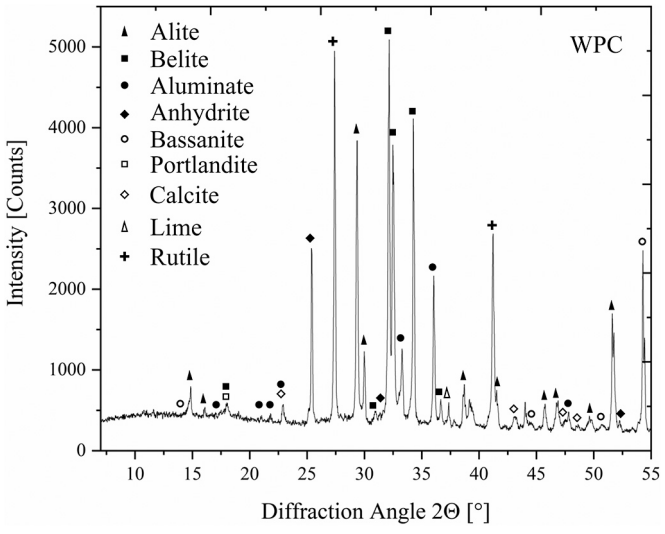

Fig. 1. Results of XRD of the raw white Portland cement.

Table 2
Composition and compressive strength after 28 days of the investigated samples.

		WPC	MC040	MC040MK
w/b		0.50	0.40	
Type of binder		CEM I white cement	CEM I gray cement	
Cement	kg/m^3	455	455	318.5
Metakaolin		–	–	136.5
Water		228	182	
Aggregates (quartzitic)		1593	1771.5	1771.5
0.0–0.25 (quartz powder)		279.3	–	
0.1–2.00		813.7	823.7	
2.0–8.00		–	947.8	
$f_{c,28d}$	N/mm^2	52.0[a]	79.6[b]	82.3[b]

[a] Tested according to DIN EN 196–1:2016.
[b] Tested according to DIN EN 12390–3:2009.

depth starting from the specimen surface. The thin sections were embedded in fluorescent as well as non-pigmented epoxy resin and ground to a thickness of 25 µm, polished and covered.

For the Proof-of-concept, testing of the concrete specimens was reduced to ^{1}H NMR measurements and phenolphthalein tests to correlate the determined carbonation depth or area affected by carbonation respectively. The investigations of the concretes were carried out on slabs of 100 × 100 × 50 mm^3 which were stored under damp cloth for 24 h after fabrication followed by water storage for further 6 days. After water storage the samples were dried at 60 °C for 7 days. The accelerated carbonation was conducted at a 3 %-CO_2-atmosphere at (21 ± 2) °C and (65 ± 5) % relative humidity for 90 days.

2.2. Methods

2.2.1. Single-sided ^{1}H NMR measurement

The relaxometry measurements were carried out using a single-sided ^{1}H NMR MOUSE from Magritek, which allows a maximum measurement depth of 25 mm and a radio-frequency (rf) of 13.12 MHz (see Fig. 3) [34]. A CPMG measurement sequence was selected for measurement by single-sided ^{1}H NMR, which allows the acquisition of a depth profile in specified step sizes. In the experiments, a total of 21 measuring depths were measured at a step size of 500 µm up to a measuring depth of 10 mm. Each of the 21 depths was measured using 1024 scans and a number of 200 echoes with an echo time of 0.158 ms and a recycle delay of 500 ms for a measurement time of 3 h. During the CPMG sequence the pulse length of the 90° as well as the 180° degree pulse was 10 µs to maintain the excited bandwidth and therefore the size of the sensitive volume while the amplitude of the pulses was changed by amplifying the 180° by 6 dB [35]. This measurement sequence was repeated 10 times per depth automatically instead of measuring one long experiment to minimize the risk of data loss. The same parameters were used for the measurement of the concrete samples.

The repetition of the measurement sequence allows a reduction of the scatter of the signal and results in an increased signal-to-noise ratio (S/N) from 45.7 to 237.7. The S/N was calculated by the amplitude of the first echo divided by the standard deviation of the last 20 echo amplitudes. Fig. 3 shows the difference of the measurement signal of a single measurement sequence compared to a signal, which was averaged from 10 measurement sequences. The magnified section of the raw data reveals the improvement of the data through averaging multiple experiments. With regard to the evaluation of the measurement signal with respect to the pore structure, which is based on a multi-exponential fit of the measurement signal, this methodology offers the possibility of a significantly more reliable result compared to a single measurement.

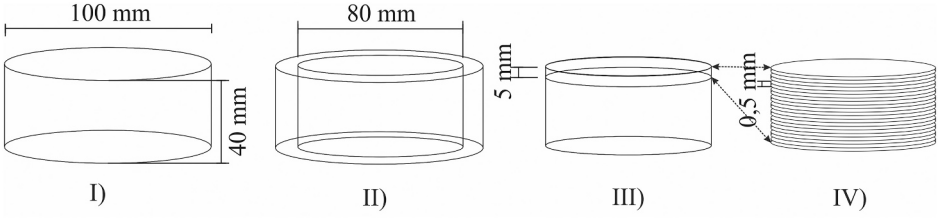

Fig. 2. Scheme of the preparation of the TGA and XRD samples by overdrilling a disk of the WPC (I) with a smaller diameter (II) followed by separating (III) and depth-graded partial grinding in 500 µm steps (IV) of the first 5 mm of the sample surface.

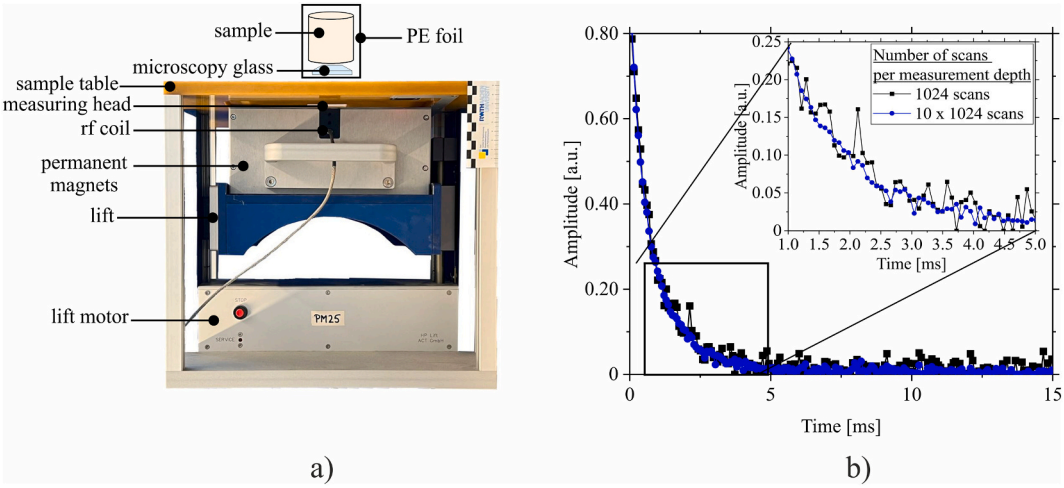

Fig. 3. a) Single-sided ^{1}H NMR MOUSE Type PM25 (Magritek) with a maximum measurement depth of 25 mm b) improved Signal-to-Noise by averaging 10 experiments with 1024 scans each (right).

The averaged measurement signals of each measurement depth in the form of exponential decay curves were evaluated using the evaluation routine according to [36], in which the signal is fitted using 4 individual exponential functions according to

$$A(t) = \sum_{i=1}^{4} A_j \left(e^{\frac{-t}{T_{2,i}}} \right) \quad (1)$$

where A corresponds to the amplitude of the signal and $T_{2,i}$ to the relaxation time of the corresponding mode. The fit is obtained using a non-negative linear least-square algorithm. Another method for evaluating the data is the inverse Laplace transformation. However, this method requires a high quality of data, which is rarely the case in the case of CPMG measurements in an inhomogeneous magnetic field. According to [37–39], each of the four functions corresponds to one of the water classes *interlayer*, *gel*, *interhydrate* and *capillary* represented by four different relaxation times in the signal of the studied volume and provides information about the pore structure of the material. The *interlayer* component allows a conclusion to be drawn about the proportion of the C-S-H phases by showing the amount of water in the interlayer of the phases which are assumed to have a layered silicate like structure [37]. The cylindrical sample of the WPC was measured in the dried and water saturated state, using the single-sided ^{1}H NMR. For the dried state, the sample was stored until equilibrium at 55 % RH. The water saturation of the samples during the investigation is defined as the water storage up to constant mass under atmospheric pressure. The signal was evaluated with respect to the different T_2 water classes according to [37,38]. To avoid overinterpreting the results due to the low S/N, fix T_2 were chosen for the analysis. Although it is expected to observe an evolution of the T_2 distribution, this approach allows us to more reliably analyze the relative distribution of the different pore classes. For the multiexponential fit in this study T_2-values of 0.15, 1.0, 3.0 and 30.0 ms, respectively, where used to obtain the different water classes. The proportion of the different water classes in percent was calculated by normalizing the amplitudes of the different T_2 to the maximum amplitude of a measurement of pure water.

2.2.2. Chemical analysis

For validation of the ^{1}H NMR method, further investigations were carried out to characterize the carbonation progress on naturally carbonated WPC. For the phenolphthalein test, the carbonation depth d_c^{pH} was determined according to [6]. A naturally carbonated drillcore was cracked in the middle and a 1 % phenolphthalein solution was applied on the fresh broken cross section. To obtain the carbonation depth, the thickness of the uncolord edge of the cross section was measured 24 h after the application of the phenolphthalein solution. The value for d_c^{pH} was obtained by measuring the uncolored edge at three locations, according to the central points of the division of the edge length into quarters. The same procedure was carried out on the concrete samples after accelerated carbonation. To verify the standardized method for the determination of the carbonation depth of the mortar, the thickness of the uncolored edge was calculated in every point over the full length of the air side, which was also used for the measurement according to the standard. The thickness was calculated using the image analysis software ImageJ by tracing the outer edge and the edge of the uncolored edge in the direction of the sample core with a segmented line. The subtraction of the line's pixel coordinates yields the distance between the lines which then was converted into µm.

In case of the WPC and in addition to the phenolphthalein test, carbon-sulfur analysis (CSA) and thermogravimetry (TGA) were performed. Thermogravimetric analysis was carried out on the powder samples which were also used for the CSA in a depth-graded manner. The TGA was carried out using a METTLER TOLEDO TGA/DSC 1 Stare System thermo balance at a temperature range of 30 to 890 °C and a heating rate of 10 K/min in a nitrogen atmosphere. To calculate the proportion of the different phases, the mass loss in specific temperature ranges was assigned to different components of the sample based on [40]. From 0 to 400 °C the mass loss can be assigned to water bound in the C-S-H, AFm and AFt phases while the mass loss between 400 and 500 °C results from the decomposition of Portlandite. In the range from 500 to 800 °C the carbonates are decomposed. No distinction between the different carbonate polymorphs was made. For the CSA, the Carbon-Sulfur Analyzer CS2000 manufactured by Eltra was used. The sample was heated up to 2000 °C in an induction stove to quantify the released carbon dioxide (CO_2) and sulfur (SO_3) using an infrared gas analyzer.

2.2.3. Microscopy

The investigation of the thin sections of the WPC was carried out by light microscopy and scanning electron microscopy (SEM). For the SEM analysis, an uncovered thin section was coated with a 3 nm carbon layer under vacuum. The back scattered electron (BSE) images were taken, using a Zeiss Supra 55 scanning electron microscope. The working distance was set to 8.5 mm using an operating voltage of 15 kV. The used magnification was 100 x resulting in a resolution of 2048 × 1536 pixel.

The covered thin section was examined using a light microscope Olympus BX 53 M equipped with an Olympus DP 23 camera and an automated table.

3. Results

3.1. Subdivision of the carbonated area based on ^{1}H NMR

In the phenolphthalein test the naturally carbonated WPC sample which were measured with the single-sided ^{1}H NMR shows an uncolored edge, indicating carbonation in this area after natural carbonation. Starting from the surface, the carbonation depth d_c^{pH} was 0.57 mm in the case of the WPC. This value was obtained by averaging the carbonation depth measured on three different locations as shown in Fig. 4, according to the standard [6]. The minimum carbonation depth is 0.32 mm and the maximum carbonation depth is 0.74 mm The other three sides show a carbonation depth apparently twice as high as a result of the core drilling process. As comparison to the standard, the mean carbonation depth was calculated based on the penetration depth profile which is shown as an overlay on Fig. 4a. The calculation results in a mean carbonation depth of 0.87 mm with a maximum at 1.73 mm and minimum at 0.32 mm.

The results of the ^{1}H NMR in Fig. 4b and c show the resulting distribution of the different modes of the measured water in %, referred to as water classes, as a function of the measurement depth, for a dried sample (4b) and re-saturated (4c). Starting from the sample surface, the first 0.5 mm give a mixed signal due to irregularities at the surface of the sample. Apart to the deviating signal of the first 0.5 mm, the overall signal, referred to as *total*, represents the amount of water present in the measurement volume. The *total* curve shows a lower water content up to a measurement depth of 2.5 mm which was assigned to the *NMR carbonated Zone A*, including d_c^{pH}. The *Zone A* based on ^{1}H NMR is connected to the structurally non-altered area referred to as *NMR non-carbonated Zone B* which is characterized by a higher water content and by the uniform *total* signal, which can be assumed to represent the bulk structure of the sample.

In addition to the total water content, the ^{1}H NMR signal can be analyzed to determine the different water classes present in the sample. Based on the results of [27], four different classes can be distinguished. It must be clarified that only some bound water can be measured by ^{1}H NMR using CPMG, which is based on the fact that the relaxation times (T_2) of crystalline bound water for most minerals (e.g. Portlandite, Ettringite) are too short to be detected. For this reason, previous research often refers to the different water classes as pore types of increasing size [27,28], according to the order of their appearance in Fig. 4.

As seen in Fig. 4c in the *NMR non-carbonated Zone B* (>3 mm deep), the water detected is mainly present in the *gel* class, followed by the

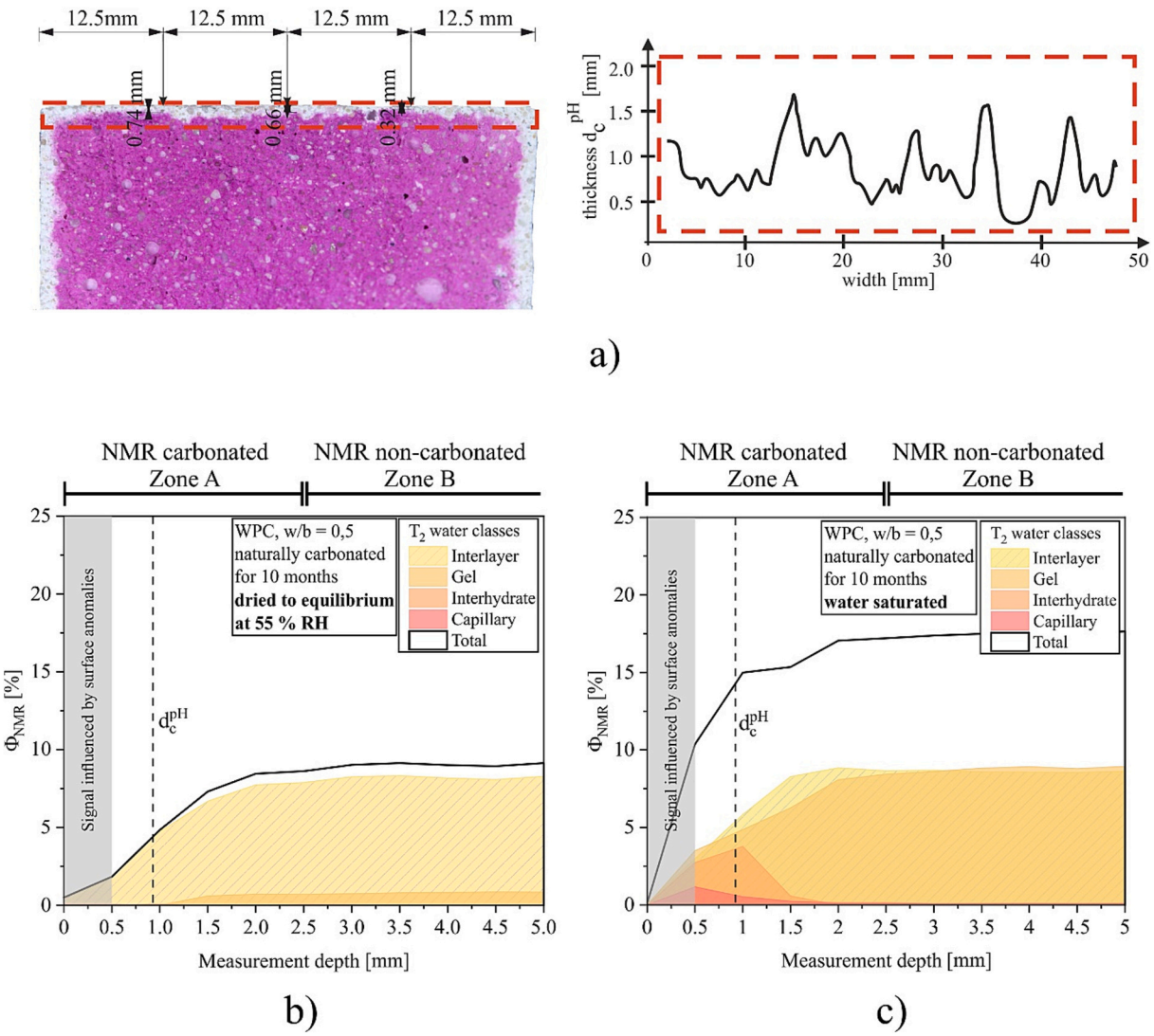

Fig. 4. a) Carbonation depth over the sample cross-section as an overlay compared to the measuring points to calculate the carbonation depth and the results of the Single-Sided ^{1}H NMR on naturally carbonated WPC sample in the dried (b) and water saturated state (c).

interlayer class, which refers to the space between the layers of calcium silicate hydrates (C-S-H). The *interhydrate* and *capillary* classes were not detected in *Zone B* of the sample. In comparison, the *NMR carbonated Zone A*, is dominated by a coarser structure. The coarser structure results from the detected classes referred to as *interhydrate* and *capillary* describing larger pores.

The measurement of the dried sample shows that the measurable water is mainly present in the *interlayer*. The *interhydrate* and *capillary* component is not measurable which indicates that this type of pore is mostly dry in this system. Compared to the water saturated sample, the *total* signal of the dried sample also shows a characteristic progression of the curve regarding the carbonation depth. Also, the proportion of the water present in the C-S-H in the dried state allows the distinction of *Zone A* and *Zone B*. As shown in the chemical analysis (Section 3.2) the change in the NMR signal is assigned to carbonation rather than only drying due to the significant correlations between the depth at which chemical and physical changes typically attributed to carbonation were observed. Some of these changes are also due to the inherent drying that occurs during carbonation as shown in previous publications [20,41,42]. The boundary of *Zone A* to *Zone B* was set in the area that shows a change in the finer structure (*gel*) without simultaneously coarsening of the structure.

For the application of the single-sided ^{1}H NMR as a non-destructive method for measuring the carbonation depth on buildings, the ability to measure non-water-saturated samples is a requirement, since building components cannot be guaranteed to be saturated.

3.2. Characterization of the areas

3.2.1. NMR carbonated zone and NMR non-carbonated zone

The *NMR carbonated Zone A* is characterized by a coarser structure as observed in the ^{1}H NMR results and confirmed by microscopy. A darker colored cement paste can be observed in *Zone A* of the thin sections in Fig. 5. This is due to the precipitation of carbonates as a result of carbonation, which is accompanied by a decrease in the overall porosity that leads to a reduction of the transmitted light. In the SEM-BSE image (Fig. 5b), the cement paste matrix in *Zone A* shows a more homogenous matrix compared to the *NMR non-carbonated Zone B* which consists of less dense components to a higher proportion, represented by lower gray values.

Fig. 6 and Fig. 7 present the results from the chemical analysis. In both the TGA and the CSA measurements, we can observe that the amounts of carbonates (or total CO_2) decrease as a function of the depth. In particular, two observations are significant: 1) the content of carbonates is not constant in *Zone A*, indicating that the carbonation process is still ongoing; and 2) the content of carbonates is not constant in *Zone B*

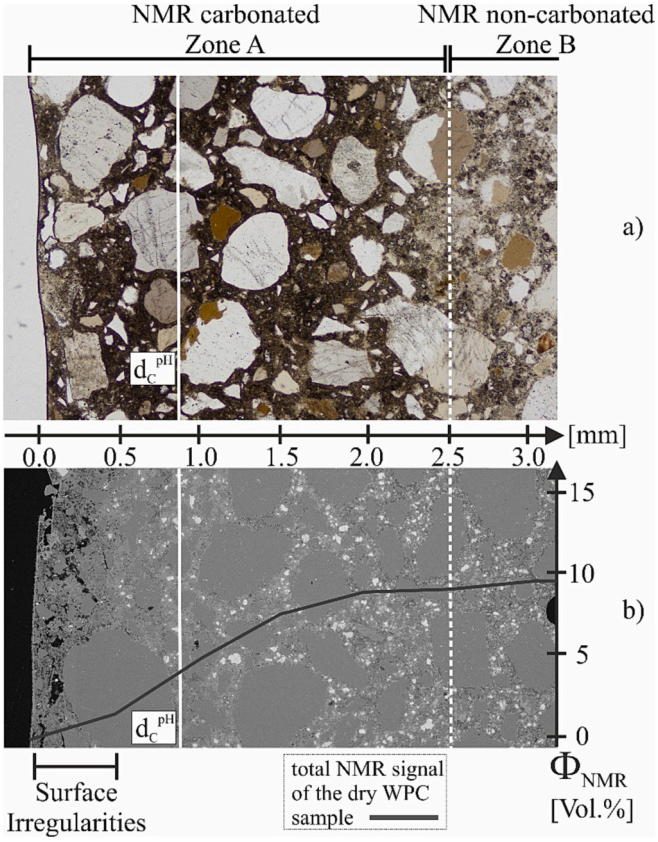

Fig. 5. Overview images taken by light microscopy (a) and SEM-BSE (b) showing the cross section of the naturally carbonated WPC with highlighted subdivision of *Zone A* and *Zone B* area and the area of surface irregularities based on the NMR results as well as the carbonation depth by phenolphthalein.

indicating that CO_2 penetrated further than the carbonation depth d_C^{pH}. Similarly, the portlandite content determined by TGA increases in *Zone B*. Although it is almost constant in *Zone A*. On the other hand, the bound water up to 400 °C is decreasing in *Zone A*, but near-constant at maximum value in *Zone B*. This indicates that in *Zone B*, the portlandite is the main buffering phase but in *Zone A*, the other hydrates (C-S-H-, AFm, AFt) are carbonating even though Portlandite is not fully depleted. This analysis is confirmed by the NMR results showing a depletion of the C-S-H interlayer in *Zone A*. The sulfate content is also decreasing (Fig. 7) in this layer. It is consistent with the results of [8,40] which shows a similar segregation of sulfate and was related to the carbonation of ettringite. The SO_3 peak in *Zone A* could be attributed to excess ettringite precipitation near the carbonation front [8]. From this interpretation, it is logical that the phenolphthalein front is present in *Zone A* as it requires most cement hydrates to be carbonated to reach a pH < 9 [40].

Based on the additional, chemical characterization by TGA and CSA the width of the *NMR carbonated Zone A* was enlarged by combining

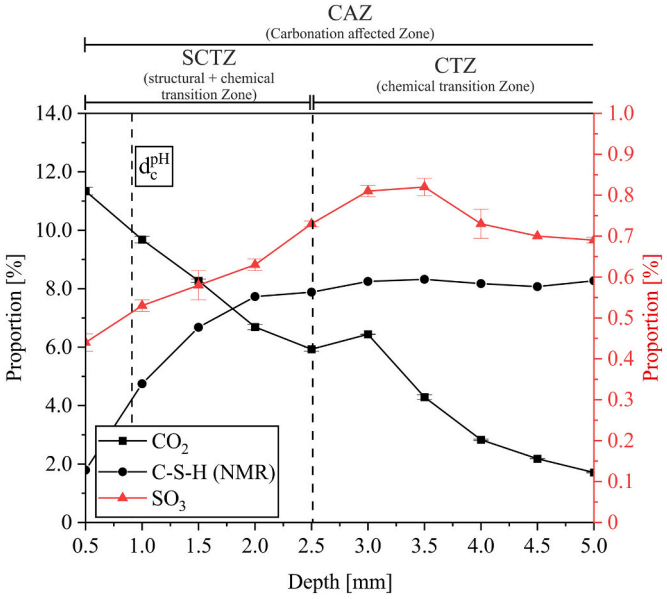

Fig. 7. CO_2 and SO_3 profiles measured by CSA with indicated carbonation depth by phenolphthalein test and C-S-H profile by ^{1}H NMR measurement in the dried state.

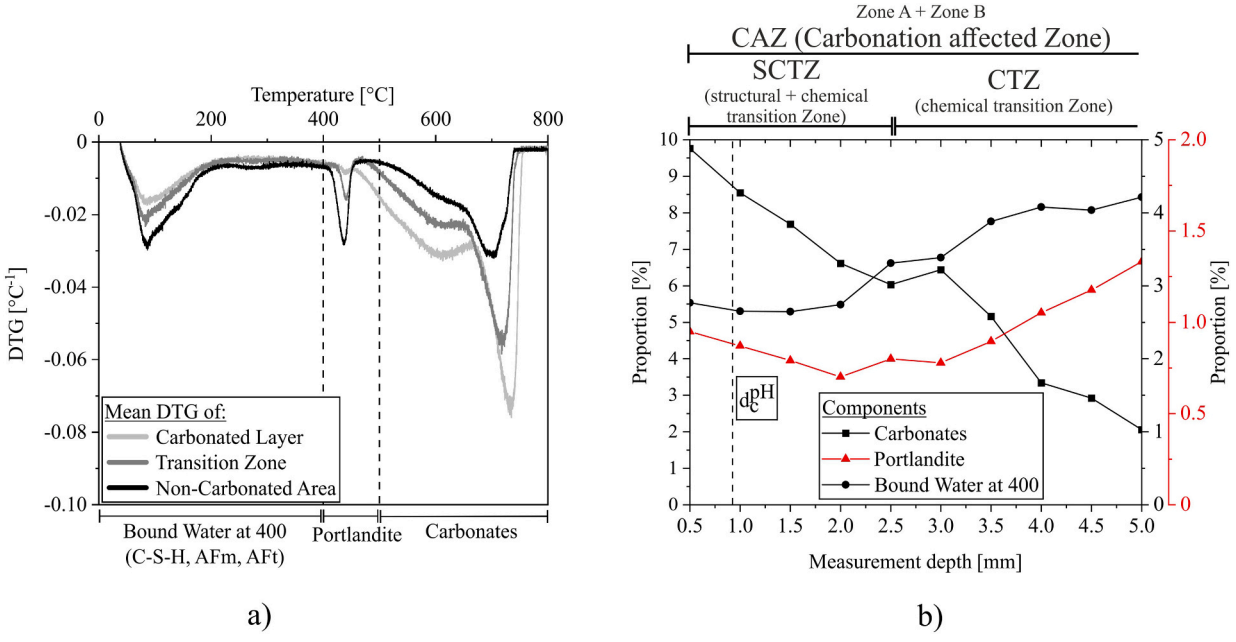

Fig. 6. Results of the TGA (a) and the derived proportion of the different components (b).

both zones, giving the *carbonation affected zone (CAZ)*. The NMR MOUSE can only detect large structural changes, and therefore, some early carbonation are not detected, even though they can be measured by chemical analysis. This is due to the varying content of the different components at depths higher than the first assumed boundary of *Zone A* and *Zone B*. Further, the *CAZ*, which now at least extends to a depth of 5 mm of the investigated sample, is divided in two separate zones, a *chemical transition zone (CTZ)* and a *chemical/structural transition zone (SCTZ)*. The *chemical transition zone* is characterized by a constant distribution of the different water classes by ^{1}H NMR and a varying distribution of the different components given by TGA and CSA. The *chemical/structural transition zone* shows a varying structure as well as a varying distribution of the different phases. Overall, the results of the chemical and the structural analysis give reason to define a fully carbonated area. In the first assumption, this would be characterized by a constant structure and by constant ratios of the individual phases. However, this is not the case in any of the samples examined.

3.2.2. Transition between CTZ and SCTZ

The additional subdivision of the *CAZ* into two separate Zones represents the different phases of the carbonation process. From the ^{1}H NMR results (Fig. 4) the transition of the *CTZ* to the *SCTZ* is related to the apparition of interhydrate and capillary pores, and the decrease in the gel pore and interlayer volume. It can also be observed in the optical microscopy results (Fig. 5) with a gradual shift towards a darker color. According to our interpretation of the *CTZ* and *SCTZ*, this transition corresponds to the area where portlandite finishes carbonation while the other hydrates (C-S-H, AFm and AFt) starts carbonating. The length of this area is attributed to the heterogeneity observed in Fig. 5 as well as the low water content as observed by NMR (Fig. 4).

The comparison of ^{1}H NMR and TGA results can be used to investigate in more details the order of carbonation. Fig. 8 presents the correlation between the ^{1}H NMR, the TGA and the CSA results. The carbonate content by CSA and TGA agrees well. However, ^{1}H NMR and TGA results deviate significantly in the *SCTZ*. Fig. 7 also indicates that SO_3 decrease significantly in this layer. This would indicate that after portlandite, the main phase to carbonate is the ettringite (initial ettringite, and secondary ettringite from the excess sulfates in the non-carbonated layer).

4. Measurements on concrete samples

For checking whether the results of the investigation of the carbonated WPC can be transferred to other cement-based building materials, ^{1}H NMR measurements were conducted on accelerated carbonated concretes as described in Section 2.

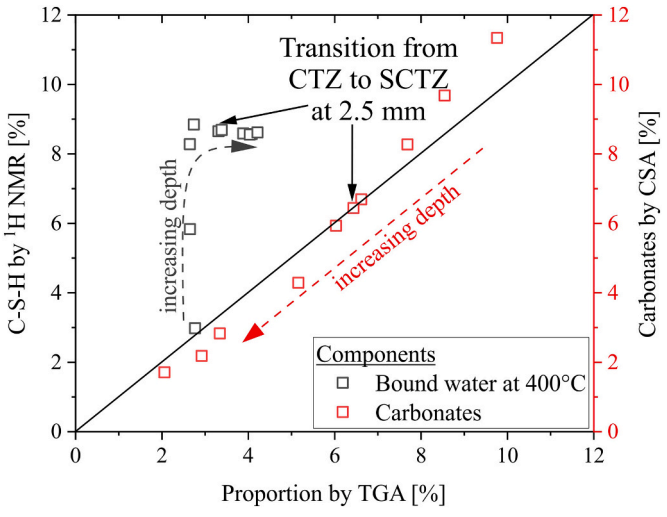

Fig. 8. Correlation of the phase proportions resulting from the different analysis showing the sensitivity of the different methods regarding structural and mineralogical phases through carbonation.

The two concretes were measured before and after accelerated carbonation after water-saturation. The derived Φ_{NMR} signals as a function of depth are shown in Fig. 9. The assumptions derived from the investigations of the WPC can be applied to the two concrete types. Although the aggregate grain size causes a coarsening of the overall structure, the decrease in porosity with a simultaneous increase in larger pores resulting from the carbonation process in the hardened cement paste can be understood from the ^{1}H NMR results. The superposition of the results of the phenolphthalein test with the results of the depth-graded ^{1}H NMR measurements on the two concretes before and after accelerated carbonation shows the characteristic course of the change in microstructure as a function of depth derived from Fig. 10. Both concretes show a decrease of the total porosity in the *SCTZ*, which is accompanied by a decrease of the *interlayer* signal assigned to the C-S-H phases.

At the same time, an increase in the *interhydrate* and *capillary* signals assigned to the larger pores was observed. These results agree with the results of the ^{1}H NMR measurements on the carbonated WPC. Likewise, a transition from *CTZ* to *SCTZ* could be determined for both concretes, which, in the case of the MC040 concrete, exceeds the maximum measurement depth of the single-sided ^{1}H NMR and a measurement of the *CTZ* area was not possible. Compared to this, the concrete with a 30 % substitution of the cement with metakaolin (MC040MK) after accelerated carbonation for 90 days, shows a curve characterized by two plateaus. The plateaus represent the *SCTZ* in the near-surface region up to a depth of 4 mm and, on the other hand, the *CTZ* area from a depth of 6.5 mm. A comparison of the different signal components also shows a shift towards a coarser microstructure in the *SCTZ*, which is mainly characterized by an increase in the measured signals of the *interhydrate* and *capillary* components. At the same time, there is a decrease in the water bound in the *interlayer* component, which represents the C-S-H phases in the microstructure. Overall, the ^{1}H NMR results of the carbonated concretes differ from the initial distribution of the water classes within the maximum measurement depth before accelerated carbonation. Therefore, the transition from the *CAZ* to the *Bulk* was not determined.

The correlation of the ^{1}H NMR results with the phenolphthalein test also results in a deviation of the determined depth related progress of the carbonation. However, the difficulty of the determination of d_c^{pH} due to the aggregate grain size should be taken into account here. It leads to a fuzzy boundary curve of the phenolphthalein test.

5. Discussion

Understanding the structural and mineralogical changes through carbonation is fundamental to optimize the choice of repair measure to prevent corrosion of the steel reinforcement. This paper provides insights into the carbonation process using the non-destructive method single-sided ^{1}H NMR validated by further chemical and mineralogical investigation techniques.

5.1. Comparison of the carbonation progress by ^{1}H NMR and phenolphthalein

From the ^{1}H NMR measurements on white cement mortar (Fig. 4) and the two different concretes (Fig. 9) it can be observed that single-sided ^{1}H NMR yields a carbonation profile while phenolphthalein gives you the state of carbonation at a certain point (d_c^{pH}, pH < 9). The carbonation profile by ^{1}H NMR is divided into the areas: 1) *Carbonation affected Zone (CAZ) and* 2) *Bulk* while the CAZ is subdivided into a Zone of a) chemical transition (*CTZ*) and b) structural and chemical transition (*SCTZ*). In the present study d_c^{pH} mainly lies within the *STCZ* layer while the *CTZ* is not always included in the measured carbonation depth by phenolphthalein. Furthermore, the determination of d_c^{pH} is limited in its

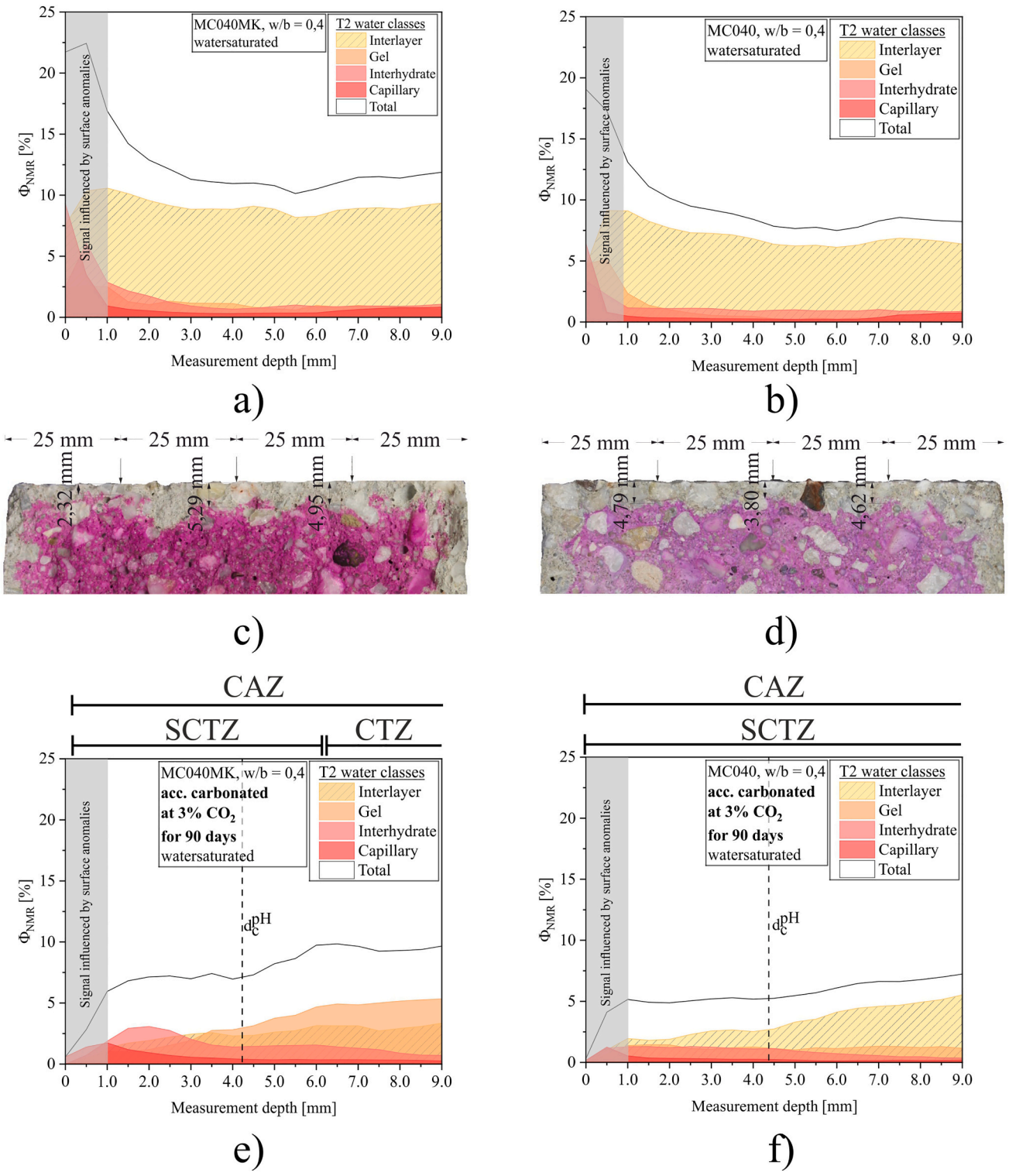

Fig. 9. Results of the Phenolphthalein test (c + d) and ^{1}H NMR measurements on non-carbonated concretes (a + b) and the same concretes carbonated under accelerated conditions (3 % CO_2) for 90 days (e + f).

accuracy by aggregates in the system and by the number of measuring points which can be avoided by measuring d_c^{pH} using image analysis as shown in Fig. 4a). The impression that the carbonation depth by phenolphthalein underestimates the progression of the carbonation should not be generated by these results. In case of steel reinforced structures, the phenolphthalein test enables the detection of the depth in which the pH of the pore solution is lower than the value needed for the passivation of the steel reinforcement. Based on this depth, the progression of the carbonation can be calculated to remaining useful life of a building structure. However, the results by single-sided ^{1}H NMR yield further information about the structural changes by carbonation not only at d_c^{pH} but also at higher depth. With it, the course of the carbonation reaction leading to the drop in pH < 9 of the respective material can be determined. In case of the investigated materials, this drop lies in the area where the coarsening of the structure begins at the boundary of the *CTZ* to the *SCTZ*. Here, the structural change during

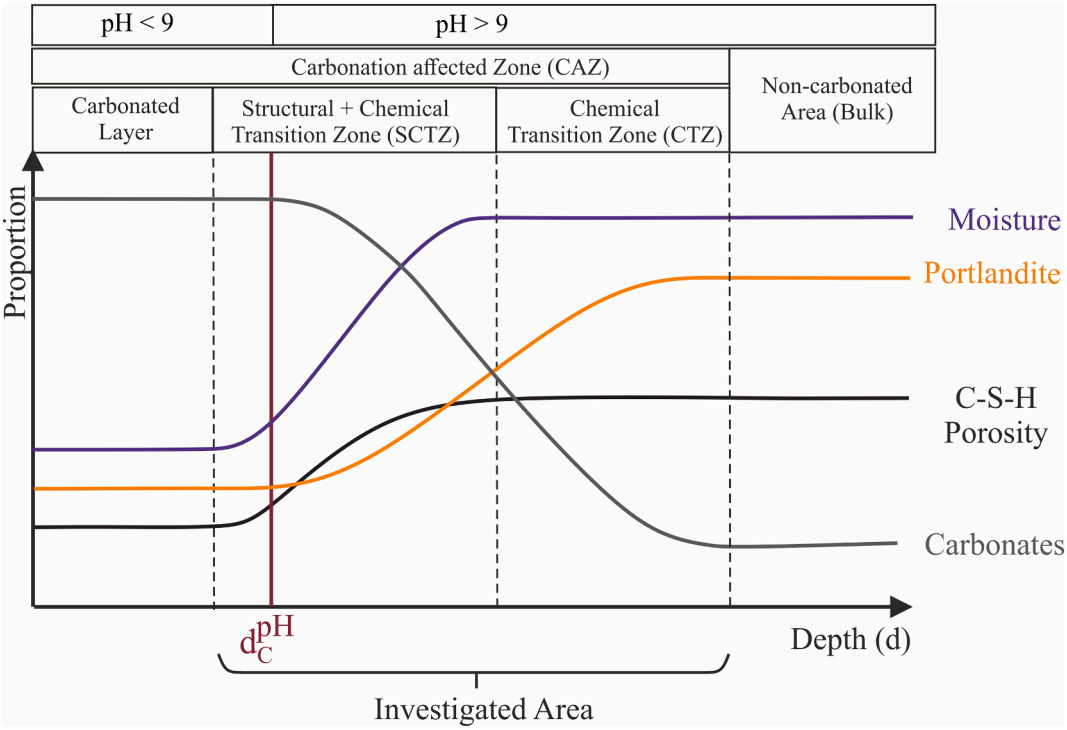

Fig. 10. Comparison of the effects of carbonation on the different structures in cement-based materials derived from different analysis methods.

carbonation of the investigated materials causes a shift in pore sizes towards larger pores with a simultaneous decrease in the overall porosity (Φ_{NMR}). These results are consistent with those of [20,22] where an increase in larger pores as a result of carbonation of cement-based materials was observed by ^{1}H NMR and mercury porosimetry (MIP). To yield a more precise characterization of the reactions leading to the drop of pH < 9, samples of one material with different carbonation depth can be analyzed.

5.2. Structural and mineralogical changes through carbonation by different techniques

Next to ^{1}H NMR and phenolphthalein, the carbonation progress of the white cement mortar was investigated using chemical analysis like CSA and TGA. Fig. 10 comprises the results of the different techniques.

Accordingly, there is a certain amount of CO_2 which can be bound in form of carbonates in the sample before the C-S-H of the cement paste gets decomposed through decalcification. By this decalcification, the concentration gradient between the hardened cement paste and the pore solution resulting from the depletion of calcium, is counteracted. This reaction is accompanied by the release of water and a decrease in the volume of the reaction product, which leads to an increase in the larger pore sizes. The overall decrease in pore space is a result of the precipitation processes of $CaCO_3$ during the carbonation reaction, which settles in the space between the hydration products of the cement.

Based on the observation by ^{1}H NMR, that the carbonated layer is characterized by a coarsening of the structure due to the degradation of the C-S-H and thus a shift in the proportion of semi-crystalline bound to free and physically bound water, the interface between the transition zone and the carbonated layer can be understood as a drying front. This drying front at around 1.5 mm is created by the release of the capillary water until the water vapor pressure is minimized. Therefore, a higher proportion of larger pores results in a lower water content in an environment characterized by humidity below the water vapor capacity of the air. The lower water content in this area as measured with ^{1}H NMR result in a non-local equilibrium carbonation front which is shown by the diffusive carbonation front. This assumption is confirmed by the results of ^{1}H NMR measurements on a dried sample, also shown in Fig. 4, which were conditioned in the same way as the samples measured in the water saturated state during the manufacturing process. The measurement shows that the total signal consists mainly of the signal of the water semi-crystalline bound in the *interlayer*-space. The change in the slope of the *total* signal agrees with that of the *total* signal of the water saturated samples. This agreement leads to the assumption that the carbonation depth could be measured on dried samples, which is important for the application of the ^{1}H NMR on site.

5.3. Requirements and limits for measuring carbonation by single-sided ^{1}H NMR

Requirement for the application of the single-sided ^{1}H NMR as a non-destructive tool for measuring the Carbonation affected Zone (*CAZ*) on site is that the carbonation depth lies within the maximum measurement depth of the NMR device. In this study, the NMR MOUSE PM25 enables a measurement up to a depth of 25 mm. According to [43], the concrete cover of steel reinforced components varies dependent on the exposure class and can be up to 50 mm. Although a detailed characterization of the structure based on the different types of bound water is not possible on dried samples, the *CAZ* could be determined in a non-destructive way using the total water content.

6. Conclusion

It is the aim of this paper to give further insight into the carbonation process of cement-based materials by the combination of different investigation techniques. For that, the single-sided ^{1}H NMR was tested as a non-destructive method to determine the carbonation progress. A comparison of the results of the different techniques among each other allows a deeper understanding of the results.

The described investigations and the listed results show that with the help of single-sided ^{1}H NMR, the *CAZ* can be determined non-destructively. The following results can be summarized:

- The ^{1}H NMR offers the possibility to determine not only the depths but also the structural and mineralogical changes as a result of carbonation.
- The progress of the carbonation could be measured on water saturated samples as well as on dried samples.
- A comparison of the results with the currently used, destructive method of the phenolphthalein test for determining the carbonation depth showed that the structural changes as a result of carbonation do not follow a sharp boundary, as the phenolphthalein test suggests. The Phenolphthalein test therefore shows one point on the carbonation profile given by the ^{1}H NMR.
- With the aid of ^{1}H NMR, the decrease in the C-S-H phases with a simultaneous increase in the carbonates and an associated reduction in the overall porosity and coarsening of the pore structure as a result of carbonation were measured for the binders investigated.
- Materials containing alternative binders such as metakaolin could also be investigated by ^{1}H NMR with respect to their microstructure and the changes caused by carbonation.
- Combining ^{1}H NMR with other techniques (such as TGA, CSA and phenolphthalein) allows to obtain the carbonation order of the hydrates. In particular, in this system (WPC) it was observed that Portlandite carbonates first, then Ettringite and C-S-H.
- The results obtained showed a very diffusive carbonation front. It is assumed that the large heterogeneities in addition to a kinetic inhibition by low moisture content is responsible for the non-local equilibrium carbonation front. The use of ^{1}H NMR allows to better characterize the moisture content and can help better analyze the shape of the carbonation front.

Based on the results, the different states of the carbonation process can be investigated using ^{1}H NMR. For the possibility of optimizing the repair measures of carbonated concrete, the influence of the different carbonation states on the efficiency of the repair measures should be analyzed. For example, a dense structure as a result of carbonation prevents the introduction of hydroxide ions to restore alkalinity in the concrete which makes the determination of porosity limits interesting.

Further, the non-destructive determination of the carbonation depth d_C^{pH} by ^{1}H NMR is of interest. A requirement for this is the direct correlation of the structural change within the carbonation and the associated changes in the pore solution. For this purpose, carbonation progresses of varying degrees can be generated on a material and measured using ^{1}H NMR and pH indicators.

CRediT authorship contribution statement

Clarissa Glawe: Conceptualization, Data curation, Formal analysis, Investigation, Methodology, Project administration, Visualization, Writing – original draft. **Fabien Georget:** Methodology, Writing – review & editing. **Michael Raupach:** Supervision. **Thomas Matschei:** Supervision.

Declaration of competing interest

The authors declare that they have no known competing financial interests or personal relationships that could have appeared to influence the work reported in this paper.

Data availability

The data that has been used is confidential.

References

[1] G. Groves, D. Rodway, I. Richardson, The carbonation of hardened cement pastes, Adv. Cem. Res. 3 (1990) 117–125, https://doi.org/10.1680/adcr.1990.3.11.117.

[2] Y.F. Houst, F.H. Wittmann, Depth profiles of carbonates formed during natural carbonation, Cem. Concr. Res. 32 (2002) 1923–1930, https://doi.org/10.1016/S0008-8846(02)00908-0.

[3] T.A. Bier, Influence of type of cement and curing on carbonation progress and pore structure of hydrated cement pastes, MRS Online Proceedings Library (OPL) 85 (1986) 123.

[4] B. Johannesson, P. Utgenannt, Microstructural changes caused by carbonation of cement mortar, Cem. Concr. Res. 31 (2001) 925–931, https://doi.org/10.1016/S0008-8846(01)00498-7.

[5] J. Kropp, Karbonatisierung und Transportvorgänge in Zementstein, Universität Karlruhe, 1983.

[6] DIN EN 12390-10: 2019-08, Testing of Hardened Concrete-Part 10: Determination of Carbonation Resistance of Concrete at Atmospheric Concentration of Carbon Dioxide, 2019.

[7] F. Díaz-Díaz, P.F. de Cano-Barrita, F.M. Leon-Martinez, F. Castellanos, Unilateral low-field magnetic resonance measurements of carbonation depth in unsaturated and saturated Portland cement mortars, Cem. Concr. Res. 138 (2020) 106237, https://doi.org/10.1016/j.cemconres.2020.106237.

[8] F. Georget, W. Soja, K. Louise Scrivener, Characteristic lengths of the carbonation front in naturally carbonated cement pastes: implications for reactive transport models, Cem. Concr. Res. 134 (2020) 106080, https://doi.org/10.1016/j.cemconres.2020.106080.

[9] C. Cheng-Feng, C. Jing-Wen, The experimental investigation of concrete carbonation depth, Cem. Concr. Res. 36 (2006) 1760–1767, https://doi.org/10.1016/j.cemconres.2004.07.025.

[10] D.O. McPolin, P.A. Basheer, A.E. Long, Carbonation and pH in mortars manufactured with supplementary cementitious materials, J. Mater. Civ. Eng. 21 (2009) 217–225, https://doi.org/10.1061/(ASCE)0899-1561(2009)21:5(217).

[11] B. Kraft, R. Achenbach, H.-M. Ludwig, M. Raupach, Hydration and Carbonation of Alternative Binders, Corrosion and Materials Degradation 3 (2022) 19–52, https://doi.org/10.3390/cmd3010003.

[12] A. Merah, Concrete anti-carbonation coatings: a review, J. Adhes. Sci. Technol. 35 (2021), https://doi.org/10.1080/01694243.2020.1803594.

[13] G.C. Réus, M.H.F. Medeiros, Chemical realkalization for carbonated concrete treatment: alkaline solutions and application methods, Construct. Build Mater. 262 (2020) 120880, https://doi.org/10.1016/j.conbuildmat.2020.120880.

[14] Holthausen R. Schulte, M. Merkel, W. Breit, M. Raupach, Monitoring the microstructural deterioration of concrete exposed to leaching in purified water, Civil Engineering Design 4 (2022) 99–109, https://doi.org/10.1002/cend.202100051.

[15] M. Auroy, S. Poyet, P. Le Bescop, J. Torrenti, Impact of carbonation on the durability of cementitious materials: water transport properties characterization, EPJ Web of Conferences (2013), https://doi.org/10.1051/epjconf/20135601008.

[16] M. Auroy, S. Poyet, P. Le Bescop, J.-M. Torrenti, T. Charpentier, M. Moskura, X. Bourbon, Comparison between natural and accelerated carbonation (3% CO2): impact on mineralogy, microstructure, water retention and cracking, Cem. Concr. Res. 109 (2018) 64–80, https://doi.org/10.1016/j.cemconres.2018.04.012.

[17] M. Auroy, S. Poyet, P. Le Bescop, J.-M. Torrenti, T. Charpentier, M. Moskura, X. Bourbon, Impact of carbonation on unsaturated water transport properties of cement-based materials, Cem. Concr. Res. 74 (2015) 44–58, https://doi.org/10.1016/j.cemconres.2015.04.002.

[18] C. Thiel, R. Beddoe, D. Lowke, C. Gehlen, Accelerated carbonation: changes in water transport, porosity and phases of mortart due to different pressures, in: 10th fib International PhD Symposium in Civil Engineering, 2014.

[19] A. Morandeau, M. Thiéry, P. Dangla, Impact of accelerated carbonation on OPC cement paste blended with fly ash, Cem. Concr. Res. 67 (2015) 226–236, https://doi.org/10.1016/j.cemconres.2014.10.003.

[20] W. Soja, H. Maraghechi, F. Georget, K. Scrivener, Changes of microstructure and diffusivity in blended cement pastes exposed to natural carbonation, MATEC Web of Conferences (2018), https://doi.org/10.1051/matecconf/201819902009.

[21] C. Thiel, R. Beddoe, D. Lowke, C. Gehlen, Investigating the role of moisture on concrete carbonation using single-sided 1H-NMR, in: International RILEM Conference on Materials, Systems and Structures in Civil Engineering Conference Segment on Moisture in Materials and Structures, Technical University of Denmark, Lyngby, Denmark, 2016.

[22] P.F.J. Cano-Barrita, B.J. Balcom, F. Castellanos, Carbonation front in cement paste detected by T2 NMR measurements using a low field unilateral magnet, Materials and Structures (2017), https://doi.org/10.1617/s11527-017-1019-5.

[23] S.M. Nagel, C. Strangfeld, S. Kruschwitz, Application of 1H proton NMR relaxometry to building materials–a review, Journal of magnetic resonance open 6 (2021) 100012, https://doi.org/10.1016/j.jmro.2021.100012.

[24] H. Zhao, X. Wu, Y. Huang, P. Zhang, Q. Tian, J. Liu, Investigation of moisture transport in cement-based materials using low-field nuclear magnetic resonance imaging, Mag. Concr. Res. 73 (2021) 252–270, https://doi.org/10.1680/jmacr.19.00211.

[25] B. Blümich, J. Anders, When the MOUSE leaves the house, Magnetic Resonance 2 (2021) 149–160, https://doi.org/10.5194/mr-2-149-2021.

[26] A. Valori, Characterisation of Cementitious Materials by 1H NMR, University of Surrey, United Kingdom, 2009.

[27] P.J. McDonald, J.-P. Korb, J. Mitchell, L. Monteilhet, Surface relaxation and chemical exchange in hydrating cement pastes: a two-dimensional NMR relaxation study, Phys. Rev. E 72 (2005) 011409, https://doi.org/10.1103/PhysRevE.72.011409.

[28] Y.-Q. Song, Magnetic resonance of porous media (MRPM): a perspective, J. Magn. Reson. 229 (2013) 12–24, https://doi.org/10.1016/j.jmr.2012.11.010.

[29] A. Keil, J. Orlowsky, M. Raupach, Use of a mobile NMR sensor as a non-destructive measurement system in building preservation, Bautechnik 88 (2011) 741–748, https://doi.org/10.1002/bate.201101499.
[30] R. Schulte-Holthausen, M. Raupach, M. Merkel, W. Breit, Non-destructive determination of the leaching of concrete using unilateral hydrogen nuclear magnetic resonance, Bautechnik 97 (2020) 679–687, https://doi.org/10.1002/bate.202010081.
[31] R. Schulte-Holthausen, M. Raupach, A phenomenological approach on the influence of paramagnetic iron in cement stone on 2D T1-T2 relaxation in single-sided 1H nuclear magnetic resonance, Cem. Concr. Res. 120 (2019) 279–293, https://doi.org/10.1016/j.cemconres.2019.03.027.
[32] Bundesanstalt für Wasserbau, BAWRecommendation repair products-instructions for the expert planner on structure-related product characteristics and test methods, Edition 2019 (2019).
[33] M. Castellote, L. Fernandez, C. Andrade, C. Alonso, Chemical changes and phase analysis of OPC pastes carbonated at different CO2 concentrations, Mater. Struct. 42 (2009) 515–525, https://doi.org/10.1617/s11527-008-9399-1.
[34] B. Blümich, J. Perlo, F. Casanova, Mobile single-sided NMR, Prog. Nucl. Magn. Reson. Spectrosc. 52 (2008) 197–269, https://doi.org/10.1016/j.pnmrs.2007.10.002.
[35] Casanova F., Perlo J., Blümich B., Single-sided NMR. (2011) Springer.
[36] R. Schulte-Holthausen, Evaluation of the Pore Structure of Concrete Using Single-Sided 1H Nuclear Magnetic Resonance Relaxometry, RWTH Aachen, Faculty of Civil Engineering, 2019, https://doi.org/10.18154/RWTH-2019-07752.
[37] H.M. Jennings, A model for the microstructure of calcium silicate hydrate in cement paste, Cem. Concr. Res. 30 (2000) 101–116, https://doi.org/10.1016/S0008-8846(99)00209-4.
[38] H.M. Jennings, Refinements to colloid model of CSH in cement: CM-II, Cem. Concr. Res. 38 (2008) 275–289, https://doi.org/10.1016/j.cemconres.2007.10.006.
[39] A.C.A. Muller, K.L. Scrivener, A.M. Gajewicz, P.J. McDonald, Densification of C–S–H measured by 1H NMR relaxometry, J. Phys. Chem. C 117 (2013) 403–412, https://doi.org/10.1021/jp3102964.
[40] Z. Shi, B. Lothenbach, M.R. Geiker, J. Kaufmann, A. Leemann, S. Ferreiro, J. Skibsted, Experimental studies and thermodynamic modeling of the carbonation of Portland cement, metakaolin and limestone mortars, Cem. Concr. Res. 88 (2016) 60–72, https://doi.org/10.1016/j.cemconres.2016.06.006.
[41] P.J. McDonald, O. Istok, M. Janota, A.M. Gajewicz-Jaromin, D.A. Faux, Sorption, anomalous water transport and dynamic porosity in cement paste: a spatially localised 1H NMR relaxation study and a proposed mechanism, Cem. Concr. Res. 133 (2020) 106045, https://doi.org/10.1016/j.cemconres.2020.106045.
[42] F. Georget, J.H. Prévost, B. Huet, Impact of the microstructure model on coupled simulation of drying and accelerated carbonation, Cem. Concr. Res. 104 (2018) 1–12, https://doi.org/10.1016/j.cemconres.2017.11.008.
[43] DIN EN 1992-1-1: 2011-01, Eurocode 2: Bemessung und Konstruktion von Stahlbeton-und Spannbetontragwerken–Teil 1–1: Allgemeine Bemessungsregeln und Regeln für den Hochbau; Deutsche Fassung EN 1992-1-1: 2004+ AC: 2010, 2011, https://doi.org/10.31030/1723945.